Journal of
Synchrotron Radiation

ISSN 0909-0495

Received 4 May 2009
Accepted 11 September 2009

X-ray pair distribution function analysis of nanostructured materials using a Mythen detector

Richard G. Haverkamp[a]* and Kia S. Wallwork[b]

[a]School of Engineering and Advanced Technology, Massey University, New Zealand, and [b]Australian Synchrotron, Australia. E-mail: r.haverkamp@massey.ac.nz

Total scattering from nanocrystalline materials recorded on the Australian Synchrotron powder diffraction beamline has been analysed to produce atomic pair distribution functions (PDFs) for structural analysis. The capability of this beamline, which uses the massively parallel Mythen II detector, has been quantified with respect to PDF structure analysis. Data were recorded to a wavevector magnitude, Q, of 20.5 Å^{-1}, with successful PDFs obtained for counting times as short as 10 s for crystalline LaB_6 and 180 s for nanocrystalline (47 Å) anatase. This paper describes the aspects of a PDF experiment that are crucial to its success, with reference to the outcomes of analysis of data collected from nanocrystalline TiO_2 and microcrystalline LaB_6 and IrO_2.

Keywords: X-ray; total scattering; Mythen; pair distribution function; powder diffraction; nanocrystalline; amorphous.

1. Introduction

X-ray powder diffraction is a well established technique for determining the atomic structure of crystalline materials (Pecharsky & Zavalij, 2009). The technique makes use of Bragg peaks which arise from the diffraction of X-rays by the long-range periodic order of crystalline materials. The precise lattice parameters and structural characterization of such crystalline materials are thereby determined using Rietveld analysis of the Bragg peaks.

It is through understanding the structure–property relations of materials that it is possible to enhance, modify and develop new functional materials. However, gaining structural information from nanostructured materials has provided an additional challenge to powder diffraction, which suffers from limitations owing to crystallite size broadening of Bragg peaks once crystals are of the nanometre scale. Traditional powder diffraction relies on sufficient long-range periodic order to be present, which may not be the case for nanomaterials because either the particles are too small or the degree of disorder within the material is too high. An alternative approach, which is gradually being more widely adopted (Petkov, 2008), is to use the total scattering pattern, taking into account more than just the Bragg peaks. This approach is called the atomic pair distribution function (PDF) analysis technique (Egami & Billinge, 2003) or total scattering analysis.

Pair distribution function analysis enables useful structural information to be obtained from materials with broad and/or low-intensity Bragg peaks. It is particularly useful for investigation of materials with only short-range structural repeatability. The reduced atomic PDF, $G(r)$, provides information on the number of atoms in a spherical shell at a distance r from a reference atom. It gives quantitative information on the spacing of atoms in a structure and the number of atoms with this spacing. The function $G(r)$ oscillates above and below zero (when plotted against r) with positive peaks indicating distances between pairs of atoms and negative troughs indicating distances lacking atoms and therefore below the average atomic density.

A further advantage of the PDF technique is that actual bond lengths are obtained directly, compared with Rietveld analysis of powder diffraction patterns where the bond lengths that are obtained are from average atomic positions. In many cases the average and real distances are the same; however, there are structures where these differ. For example, where an atom rotates around its average position; in this case the apparent bond length determined by the average atomic position is shorter than the actual bond length determined by PDF (Tucker *et al.*, 2000). There are methods to solve such structures without using PDF analysis (Busing & Levy, 1964; Cruickshank, 1961); however, PDF analysis provides a useful alternative.

Generally, in order to achieve useful total scattering information, data need to be collected with a better signal-to-noise ratio than for Rietveld analysis (Petkov, 2008) and must be collected to high Q, preferably 20 Å^{-1} or higher. These requirements normally dictate the use of a synchrotron X-ray source or a spallation neutron source, although laboratory systems with Mo $K\alpha$ sources have been used for PDF analysis (Brühne *et al.*, 2005). With synchrotron sources, high-energy X-rays, typically in the range 40–130 keV, are used in order to achieve high Q (Brühne *et al.*, 2005; Petkov *et al.*, 2000; Chupas *et al.*, 2003).

Even with bright synchrotron sources, point by point detectors require long counting times, especially to achieve sufficient signal to noise at high angles (Brühne *et al.*, 2005). One way to improve the high Q performance and reduce counting time is to use a two-dimensional detector. The use of an image plate detector has been demonstrated to be well suited to PDF analysis (Chupas *et al.*, 2003). A further advance on image plate detectors has been the use of an amorphous silicon-based area detector at Argonne National Laboratory to achieve very rapid data collection (less than 1 s) for time-resolved PDF analysis (Chupas *et al.*, 2007*a*,*b*).

The recently built Australian Synchrotron has a powder diffraction beamline which uses a massively parallel Mythen II detector (Schmitt *et al.*, 2003; Bergamaschi *et al.*, 2009). The X-ray beam source is a bending magnet, and the beamline utilizes vertically collimating and vertically focusing mirrors in addition to a Si(111) double-crystal monochromator to condition the beam (Wallwork *et al.*, 2007).

The purpose of this paper is to demonstrate the experimental set-up required to produce satisfactory PDF results and demonstrate the sensitivity of the technique to a number of experimental variables. In addition, the suitability of the Australian Synchrotron powder diffraction beamline for collection of data for PDF analysis has been shown. Some experimental aspects which are quite specific to the type of detector in use at the beamline have also been examined.

It is intended that the work discussed here will provide a useful guide to researchers new to the field of PDF analysis, alerting them to the practical considerations of PDF analysis, through demonstration of the outcomes of total scattering analysis of data from nanostructured titanium dioxide, microcrystalline lanthanum hexaboride and nanocrystalline iridium dioxide.

2. Experimental

The Mythen II detector is a silicon microstrip detector; the Australian Synchrotron installation of the detector consists of 16 modules each having 1280 channels, totalling 20480 channels. The intrinsic angular resolution of the detector is 0.004° (with a strip pitch of 50 µm) and the detector covers a solid angle of 80° in 2θ. As the detector is modular there is a small gap between adjacent modules of around 0.2°; this is accounted for by a data collection strategy which moves the detector by ∼0.5° such that data are recorded where there was previously a gap. The readout time of the Mythen is 250 µs enabling very fast acquisition of scattering data (Schmitt *et al.*, 2003; Wallwork *et al.*, 2007). In order to achieve data collection over an angular spread greater than 80° the detector is moved accordingly; on this beamline the maximum achievable angle is approximately 160° 2θ. In the work reported here data were recorded at four nominal detector positions for each sample and set-up variable. This allowed data to be collected over the angle range 0.2° to 149° in 2θ. The upper 2θ limit for this experiment was dictated by shadowing of the diffracted beam by mechanical beamline components. In most cases, analysis of the data was carried out following merging of these histograms into one pattern with a uniform step size in 2θ (but therefore varying in Q).

An X-ray wavelength, λ, of 0.59074 (1) Å (21 keV), which is the maximum operable energy for this monochromator set-up, was used throughout the experiment. The wavelength was determined accurately through Rietveld analysis of the diffraction pattern from LaB_6. A short wavelength, in combination with recording data to a large diffraction angle, 2θ, was necessary to obtain data to high Q-space.

TiO_2 samples were prepared by hydrothermal precipitation of titanium iron chloride solutions prepared by hydrochloric digestion of NZ ilmenite, details of which will be the subject of a separate paper. IrO_2 samples were prepared by hydrothermal precipitation from $IrCl_3$ solutions at high pH (Marshall *et al.*, 2007). The LaB_6 sample was NIST standard 660a.

Samples were packed in 0.3 mm boron-rich glass capillaries, with 0.01 mm wall thickness (W. Müller, Schönwalde). Packing densities were carefully measured for all samples and ranged from 25% to 35% based on the expected solid density of crystalline forms of the materials.

In addition to scattering patterns being measured from the samples, data from the empty capillary were recorded, as were data from the vacant beam X-ray path (background). Acquisition times were varied from 10 s to 3600 s. Data were normalized to the incoming beam intensity by using the integrated ion chamber counts divided by the acquisition time. Owing to the decaying synchrotron beam the X-ray intensity variation between electron beam injections was ∼25%.

Data processing to obtain the PDF information utilized the freely available program *PDFGetX2* (Qiu *et al.*, 2004). The observed PDFs were modelled using the program *PDFgui* (Farrow *et al.*, 2007), also freely available. The book by Egami & Billinge (2003) also proved very helpful as a general tutorial in the technique and in performing the analysis.

3. Results and discussion

3.1. Processing of total scattering data

This section provides a brief review of the stages involved in data processing, particularly using data from the Australian Synchrotron powder diffraction beamline. For a detailed presentation of the procedure for PDF analysis of X-ray scattering data, refer to Egami & Billinge (2003).

The data are first normalized for incoming beam intensity, as mentioned previously, and then four diffraction patterns are merged to generate one continuous pattern over the angular range under investigation. These data are then processed to subtract the background and are plotted in reciprocal space. Representative raw and background-corrected data are shown in Fig. 1 for nanocrystalline TiO_2, where $Q = 4\pi \sin\theta/\lambda$.

The total scattering function, $S(Q)$, which is the normalized total scattering intensity plotted in Q space, is then calculated (Fig. 2*a*). While the signal-to-noise ratio looks poor at high Q, the information content is high owing partly to the large

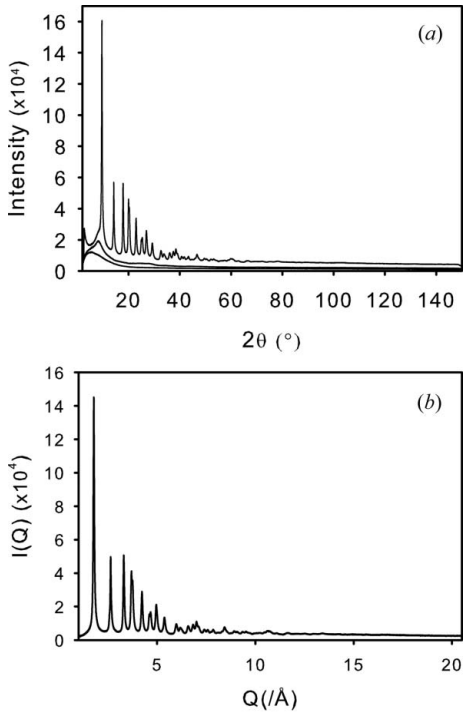

Figure 1
(*a*) Raw diffraction data for nanocrystalline TiO_2 hydrate with capillary and background (no sample) histograms shown underneath. (*b*) Background-corrected data plotted in *Q*-space. Count time 3600 s for TiO_2.

number of points at which the data are collected. A multi-point moving average could be used to reduce the noise in $S(Q)$. However, such an approach would be merely cosmetic and there is no advantage in processing the data in this way as the determination of the PDF involves a Fourier transform of these data, effectively dealing with this noise. The reduced structure function $Q[S(Q)-1]$ or $F(Q)$ is then plotted (Fig. 2*b*), and this is a useful representation to visually diagnose problems with the data or processing.

The atomic PDF, or the reduced PDF, $G(r)$, which is used here, is the Fourier transform of the total scattering intensity (Fig. 2*c*). This Fourier transform of a directly measurable quantity has a fundamental physical significance, since it is a representation of the atomic pair density. This relationship allows direct measurement of the relative positions of atoms in a solid (Egami & Billinge, 2003).

Any peaks in $G(r)$ which occur at r below the shortest interatomic distance possible for the compound analysed have no physical significance. This region is diagnostic of systematic errors in data collection or processing. Dramatic spikes in this region can be observed if, for example, capillary absorption or background are not catered for appropriately, or an incorrect sample attenuation is used in the calculation. In our plots there are often small peaks below $r = 1.5$ Å with a larger peak at $r \simeq 0.25$ Å.

3.2. The importance of recording data to high *Q*

As the process of obtaining the atomic PDF depends on a Fourier transform, data must be collected to high *Q* in order to provide sufficient information to give detailed structure at any range of *r*. Data collected over a small range of *Q* can result in ripples in $G(r)$ owing to termination errors in the Fourier transform. An inadequate *Q* range may result from data collection over a limited angular range, or through the use of insufficiently high X-ray beam energy. This is demonstrated by the data shown in Fig. 3; here the plot of $G(r)$ has been generated from data collected from nanocrystalline TiO_2 recorded to 20 $Å^{-1}$, 13.7 $Å^{-1}$ and 10 $Å^{-1}$. These are equivalent to data collected over (*a*) the full range of the instrument (140°, 21 keV), (*b*) the solid angle of the detector (80°, 21 keV), and (*c*) the solid angle of the detector but at a lower X-ray energy (80°, 15.4 keV).

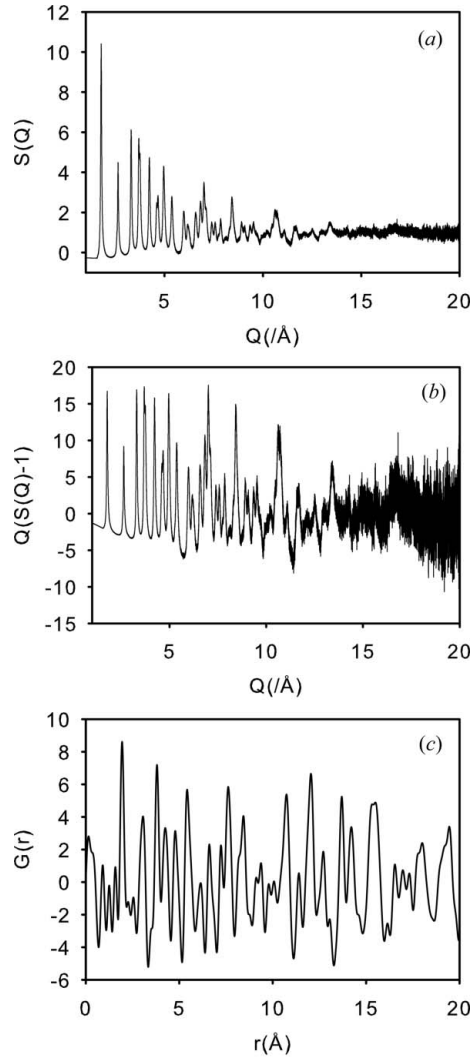

Figure 2
For nanocrystalline TiO_2 hydrate, (*a*) total scattering function, $S(Q)$, (*b*) reduced structure function $Q[S(Q) - 1]$ and (*c*) reduced PDF, $G(r)$.

It is clear that the PDF is not accurate when the data are recorded to low *Q*. The data from the nanocrystalline TiO_2 sample show spurious peaks at $r < 2$ Å, which have no physical reality, and are exacerbated when the high-*Q* region is not recorded, while the structure of the PDF loses detail across the whole range of *r* (Fig. 3).

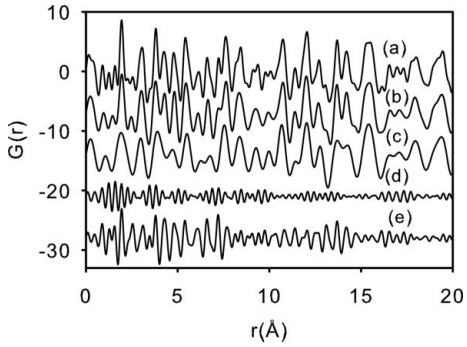

Figure 3
$G(r)$ *versus* r for Q up to (*a*) 20.5 Å^{-1} (149° at 21 keV), (*b*) 13.7 Å^{-1} (80° at 21 keV), (*c*) 10 Å^{-1} for nanocrystalline TiO_2 hydrate (99 Å crystallite size); (*d*) difference plot for (*a*)–(*b*); (*e*) difference plot for (*a*)–(*c*). The curves (*b*)–(*e*) have been offset for ease of viewing.

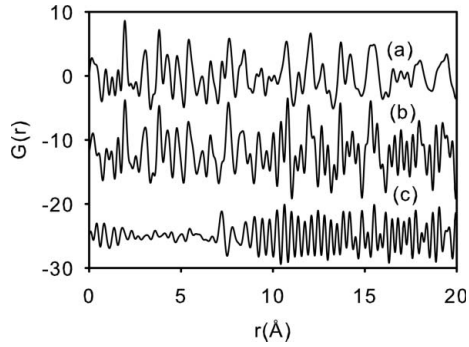

Figure 4
Reduced PDF, $G(r)$, for nanocrystalline TiO_2 (*a*) without gaps in the data, (*b*) with gaps in the data; (*c*) a plot of the difference between these. Curves (*b*) and (*c*) have been offset for ease of viewing.

If the beam energy were increased to 30 keV, then measurement to 80° provides a Q of 20 Å^{-1} without the need to move the detector significantly.

3.3. Q resolution and detection gaps in the Mythen

The Mythen II detector has an extremely good angular resolution of 0.004°. At the 21 keV energy used in these experiments, this translates to a Q resolution ranging from 0.00074 Å^{-1} at 3° to 0.00020 Å^{-1} at 149°. This excellent resolution in Q enables longer distances (several nanometres) to be probed in the PDFs of crystalline materials.

The Mythen II detector consists of 16 modules, each covering approximately 4.8° in 2θ; these are arranged such that a gap of about 0.2° occurs between each module. Normally the detector is moved by a small amount, around 0.5°, and a second histogram recorded so that the small gaps in the data are covered. However, this strategy more than doubles the collection time for a solid angle range. The effect on the PDF of retaining the gaps in the data, through collection of only one data set per solid angle, has been investigated.

A plot of $G(r)$ has been generated using data from two histograms (no gaps), and that from one histogram (with gaps) and is shown in Fig. 4. It is immediately apparent that the gaps do contribute strongly to the form of the PDF, with significant changes from 7 Å and above. Therefore, it is essential that sufficient histograms are recorded and combined to remove the periodic 0.2° gaps.

3.4. Data collection time

PDF analysis normally requires longer recording times than for Rietveld analysis. This is due to the requirement that all scattering from the sample is measured to a high signal-to-noise ratio, as it is the total scattering data that are being used, not just the relatively intense Bragg peaks. In addition, the data at high Q space (*i.e.* >10 Å^{-1}), where the scattered intensity is very low, are critical for obtaining a good PDF. However, this requirement can be prohibitive for some experiments, such as *in situ* PDF measurements, *e.g.* studies of phase crystallization. Thus, a study has been made of the significance of acquisition time to data quality, with respect to the 'crystallinity' or long-range order of the material under investigation.

For the nanocrystalline TiO_2 sample, a significant difference in signal to noise is apparent in the total scattering function, $S(Q)$, generated from data acquired for 180 s *versus* 3600 s (Fig. 5). However, the corresponding PDF shows no discernible difference in the quality of the data (Fig. 6). For the highly crystalline LaB_6, counting times as low as 10 s produced remarkably good PDF data (Figs. 7 and 8).

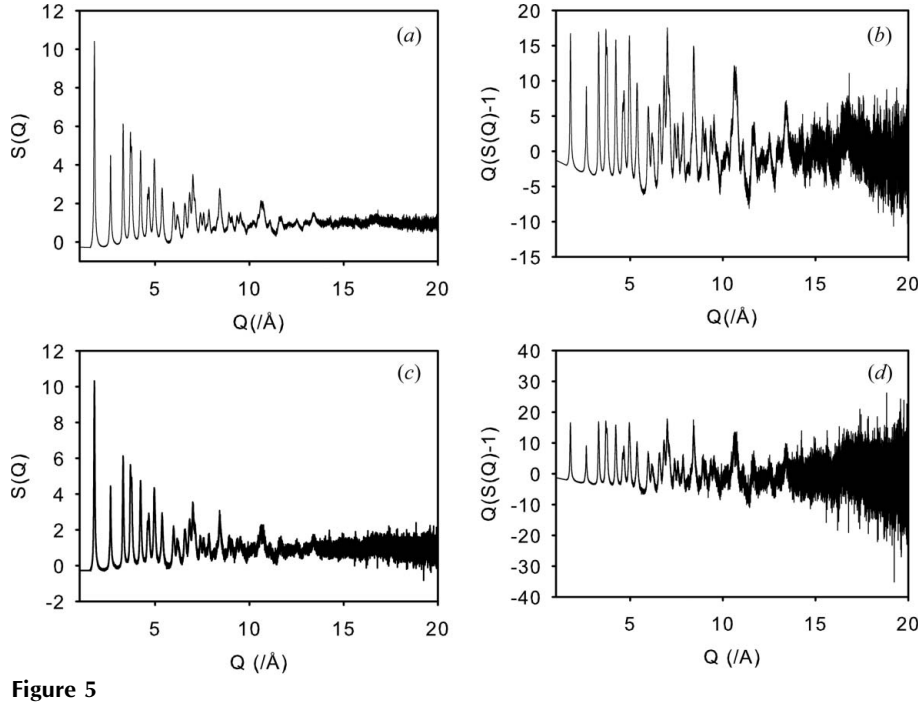

Figure 5
Total scattering function, $S(Q)$, and reduced structure function $Q[S(Q) - 1]$ for nanocrystalline anatase, where the counting times are 3600 s [(*a*) and (*b*)] and 180 s [(*c*) and (*d*)].

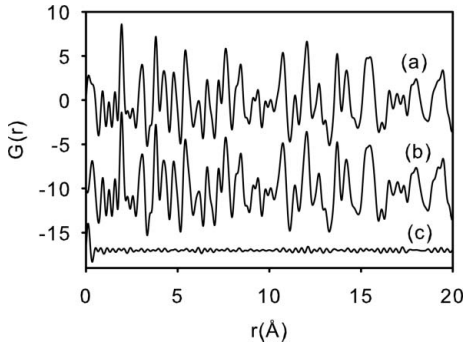

Figure 6
Reduced PDF for counting times of (*a*) 3600 s and (*b*) 180 s for nanocrystalline TiO_2, with (*c*) difference curve. The curves (*b*) and (*c*) have been offset for ease of viewing.

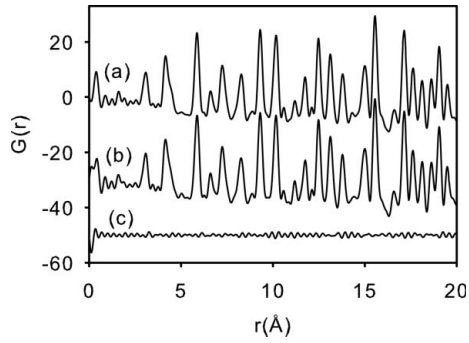

Figure 8
PDF for LaB_6 from data recorded at (*a*) 120 s and (*b*) 10 s with (*c*) difference plot also shown. The curves (*b*) and (*c*) have been offset for ease of viewing.

In order to obtain data to high Q space on this beamline it is necessary to move the detector over a large angular range which takes approximately 180 s. Thus the total minimum collection time, including data acquisition at four detector positions and the time taken to move between positions, is around 900 s and 250 s for the nanocrystalline and crystalline materials, respectively. These times may be shortened further through use of higher energy ($\geq$30 keV) and/or use of a detector covering a larger solid angle.

3.5. Detector energy discrimination

The Mythen detector has the advantage over some other systems commonly used for data collection for PDF analysis, such as image plate detectors (Chupas *et al.*, 2003), in that it has some energy resolution and therefore the ability to achieve fluorescence discrimination. This reduces the need to correct for fluorescence signal in the collected data and therefore should improve the quality of the PDF.

The Mythen detector is ideally operated with the threshold energy set at a value of half of the beam energy, according to the manufacturer's instructions (Schmitt & Bergamaschi, 2008). Thus, in this experiment the threshold would be expected to be set at 10500 eV, as the X-ray energy was 21000 eV. However, owing to the presence of fluorescence from Ir the setting of the threshold energy required further consideration. Iridium has fluorescent lines at $L\gamma_1$ 12512 eV, $L\gamma_2$ 12841 eV, $L\gamma_3$ 12923 eV, and L_β lines in the range 10510–10903 eV. Thus, according to additional instructions from the manufacturer, the threshold energy should be $\geq$3000 eV higher than any fluorescence line, and should be $\geq$3000 eV lower than the beam energy in order to avoid sacrificing too many counts. To satisfy these requirements a sample containing Ir requires a threshold energy in the range 16000–18000 eV for this X-ray energy.

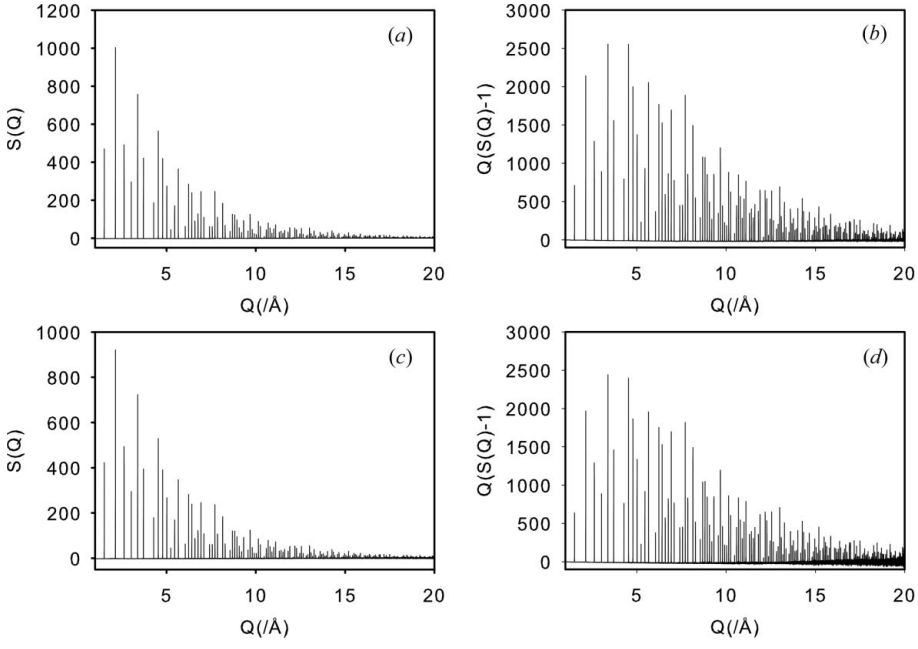

Figure 7
Total scattering function, $S(Q)$, and reduced structure function $Q[S(Q) - 1]$ for LaB_6 recorded at (*a*) and (*b*) 120 s and (*c*) and (*d*) 10 s.

The effect of setting the threshold too close to the fluorescence emission is apparent in a comparison of data recorded from IrO_2 using X-rays of energy 21000 eV, where the threshold has been set at 14000 eV and 17000 eV (Fig. 9). It can be seen in this figure that regions of the diffraction pattern are affected by fluorescence, with large, seemingly random, fluctuations in counts, usually covering an entire chip of the detector module (*i.e.* 128 channels, or $\sim$0.5°). These fluctuations probably arise because the energy discrimination of each chip in the detection module is not precisely the same as in neighbouring chips. Such fluctuations will certainly affect the quality of the PDF. Traditional Rietveld analysis of X-ray diffraction data may not be as susceptible to these imperfections, as they are small compared with the major Bragg peaks; however, it is not necessary to use such data as it is

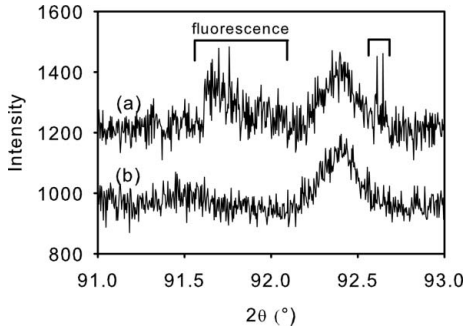

Figure 9
Raw X-ray scattering data from IrO_2 where the detector threshold was set at (*a*) 14000 eV and (*b*) 17000 eV. The incomplete discrimination of fluorescent emission, when the threshold energy is too close to the fluorescence energy, is highlighted.

a simple matter to adjust the threshold appropriately.

Compton scattering (CS) contributes to the measured total scattering profile. The amount of CS increases at higher Q, resulting in poor signal to noise. However, the energy of the CS decreases at higher Q, enabling this CS at high Q to be excluded by an appropriate selection of the detector threshold energy. A largely empirical Ruland function is applied to manage the transition from CS included at low Q to CS excluded at high Q (Egami & Billinge, 2003). A threshold energy set close to the beam energy is therefore preferable to improve the signal to noise at high Q. In this work we have used a threshold of 17000 eV for IrO_2 and 14000 eV for TiO_2 and LaB_6. However, there may be merit in increasing these thresholds to be closer to the 21000 eV beam energy to remove more of the high-Q CS, even though there would be some sacrifice in total signal intensity.

3.6. Corrections for sample container and background

Total scattering analysis, as the name implies, is analysis of the scattering from all material in the beam path. This includes contributions to the scattering pattern from air, the sample container, such as a capillary, and the sample. Therefore, care needs to be taken to remove that portion of the scattering which is due to the sample container (capillary) and scattering from the sample environment. These reference data are used during data processing. As a result, it is critical to measure scattering from the sample container and the background (sample free) under exactly the same conditions as that in which data from the sample of interest are measured. To achieve this it is necessary to avoid moving any beamline component, including the beam-stop, between these different measurements. In addition, the background-correction errors can be minimized by using containers which have a low X-ray absorption coefficient, such as capillaries of high boron content glass, kapton (polyimide) or PET (polyethylene terephthalate) (von Dreele, 2006; Reibenspies & Bhuvanesh, 2006).

During this study, data were collected from samples contained in polyimide (0.34 mm internal diameter, wall thickness 0.025 mm, Cole-Palmer, Vernon Hills, IL, USA) and compared with those collected from samples contained in borosilicate glass. There was no appreciable improvement in the quality of the PDF analysis using polyimide over borosilicate glass. Only a small difference between the intensity of the scattering pattern of the polyimide capillaries and the boron-rich glass was observed (Fig. 10). The glass capillaries gave rise to slightly less scattering than the thicker polyimide capillaries at higher Q (the region over 9 Å^{-1}).

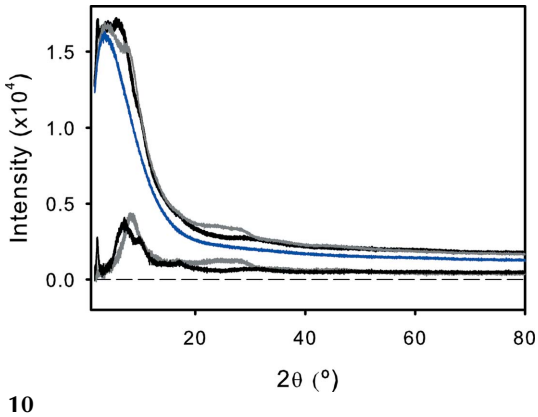

Figure 10
Scattering data from boron-rich glass capillary, 0.3 mm diameter, 0.01 mm wall thickness (top grey line); polyimide, 0.34 mm diameter, 0.025 mm wall thickness (top black line); background with no capillary (blue line or middle grey line in black and white); glass minus background (bottom grey line); polyimide minus background (bottom black line).

Corrections are also required for absorption and multiple scattering. These effects are more pronounced at the relatively low-energy X-rays used (21 keV) compared with beamlines using, for example, an 80 keV source (Petkov *et al.*, 2000). Using the *PDFGetX2* software (Qiu *et al.*, 2004), corrections can be adequately achieved for absorption and multiple scattering.

3.7. Simulation of PDF from crystal structure and fitting data to crystal lattice

Using the software *PDFgui* (Farrow *et al.*, 2007) it is possible to generate simulated PDF data for materials with known lattice structures. The simulated data may then be fit to the PDF generated from the data and allow modelling of the lattice and other parameters. This is demonstrated for the nanocrystalline TiO_2 (Fig. 11) which has the anatase structure. The literature lattice parameters for anatase, which crystallizes in the space group $I4_1/amd$, are a = 3.784, c = 9.515 Å (Horn *et al.*, 1972). Fitting the model to $G(r)$ over r from 1.6–10.5 Å shows the lattice parameters for the material studied to be a = 3.783 (2), c = 9.512 (3) Å, R_w = 26%, in close agreement with the literature. For comparison, Rietveld analysis of the pattern gives a = 3.79 (1), c = 9.51 (1) Å with R_{wp} = 4.0%. The crystallite size estimated by fitting the model to the data up to $G(r)$ of 20 Å was found to be about 47 Å. Line broadening is largely the result of small crystallite size and lattice distortions and an estimate from Scherrer line broadening of the (100) Bragg peak gives a crystallite size of about 99 Å if no broadening is attributed to lattice distortions. This crystallite size is larger than the value obtained from the PDF, although it is now well

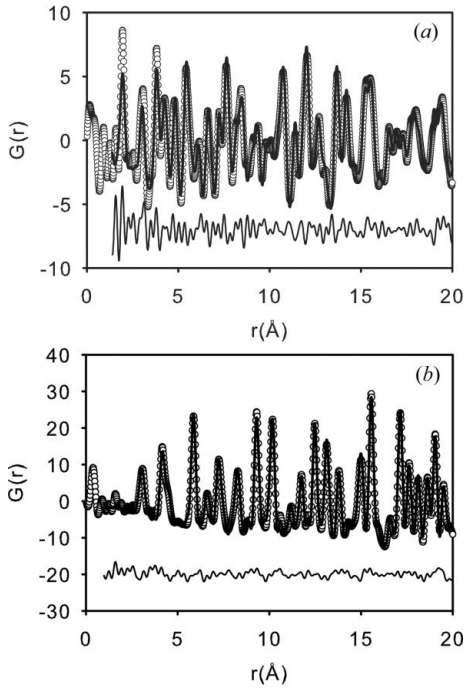

Figure 11
Reduced PDF data for (*a*) anatase showing the calculated fit (line) to the experimental data (circles) over the range 1.5–20 Å giving R_w = 26%, where the acquisition time was 3600 s; and (*b*) LaB_6 showing the calculated fit (line) and experimental data (circles), where the acquisition time was 120 s, giving R_w = 11%. Difference plots, offset for ease of viewing, are shown below each of the data curves.

recognized that the Scherrer method gives an overestimate (Le Bail, 2008).

Similarly, for crystalline LaB_6 the simulated $G(r)$ can be fit to the experimental data, and this standard material can be useful in identifying instrumental parameters needed in the fitting procedure. From this, the damping factor, *Qdamp*, which is a parameter which accounts for finite resolution in Q, is found to be very low (<0.001 Å) such that zero is a good approximation. This is a result of the very good 2θ resolution of 0.004° of the Mythen detector (which has a Q resolution of 0.00074–0.00020 $Å^{-1}$ at the energy used here).

The quality of the fit may be used to give an indication of the data acquisition time required to obtain sufficiently good data (Chupas *et al.*, 2007*b*). For nanocrystalline TiO_2, improved fits were obtained with longer exposure time (180 s, R_w = 27.5%; 600 s, R_w = 26.9%; 3600 s, R_w = 26.2%). That the gains are only slight demonstrates that short acquisition times are sufficient and perhaps even shorter times than examined here may be used. Similarly, for LaB_6 the fits with increasing exposure time show that a relatively good agreement can be achieved in 10 s (10 s, R_w = 11.9%; 30 s, R_w = 12.1%; 60 s, R_w = 11.7%; 120 s, R_w = 11.5%), thus this is a sufficient acquisition time for such highly crystalline materials. By comparison, Rietveld analysis of LaB_6 results in R_{wp} = 6.4%. As observed by other researchers (Chupas *et al.*, 2007*b*), Rietveld refinement generally reports better agreement factors than those obtained by PDF analysis.

4. Conclusions

It has been possible to demonstrate the use of the Australian Synchrotron powder diffraction beamline, using the Mythen detector for data acquisition, for pair distribution function analysis of the total scattering pattern. The data can be collected to sufficiently high Q to obtain high-quality PDF data. It has been shown that the 0.2° gaps in the data resulting from the Mythen detector need to be filled by using overlapping detector positions, as is the standard procedure on this beamline. Reasonably fast data collection is possible with no smoothing of the data required. Care must be taken to eliminate the effects of fluorescence emission, owing to the limited inherent energy discrimination of the detector. The beamline has been shown to be very well suited to PDF analysis, opening the way for studies of poorly crystalline materials and complex structural studies of materials.

This research was undertaken on the powder diffraction beamline at the Australian Synchrotron, 800 Blackburn Road, Clayton, Victoria, Australia, proposals 1159 and 1583. The views expressed herein are those of the authors and are not necessarily those of the owner or operator of the Australian Synchrotron. The NZ Synchrotron Group is acknowledged for travel funding, and the Massey University Research Fund for other research costs. We thank Dr Aaron Marshall, University of Canterbury, for the IrO_2 and for helpful discussions. We thank the anonymous reviewers for their constructive comments.

References

Bergamaschi, A., Cervellino, A., Dinapoli, R., Gozzo, F., Henrich, B., Johnson, I., Kraft, P., Mozzanica, A., Schmitt, B. & Shi, X. (2009). *Nucl. Instrum. Methods Phys. Res. A*, **604**, 136–139.
Brühne, S., Uhrig, E., Luther, K.-D., Assmus, W., Brunelli, M., Masadeh, A. S. & Billinge, S. J. I. (2005). *Z. Kristallogr.* **220**, 962–967.
Busing, W. R. & Levy, H. A. (1964). *Acta Cryst.* **17**, 142–146.
Chupas, P. J., Chapman, K. W., Jennings, G., Lee, P. L. & Grey, C. P. (2007*a*). *J. Am. Chem. Soc.* **129**, 13822–13824.
Chupas, P. J., Chapman, K. W. & Lee, P. L. (2007*b*). *J. Appl. Cryst.* **40**, 463–470.
Chupas, P. J., Qiu, X., Hanson, J. C., Lee, P. L., Grey, C. P. & Billinge, S. J. L. (2003). *J. Appl. Cryst.* **36**, 1342–1347.
Cruickshank, D. W. J. (1961). *Acta Cryst.* **14**, 896–897.
Egami, T. & Billinge, S. J. L. (2003). *Underneath the Bragg Peaks: Structural Analysis of Complex Materials.* Oxford: Pergamon.
Farrow, C. L., Juhas, P., Liu, J. W., Bryndin, D., Bozin, E. S., Bloch, J., Proffen, Th. & Billinge, S. L. J. (2007). *J. Phys. Condens. Matter*, **19**, 335219.
Horn, M., Schwerdtfeger, C. F. & Meagher, E. P. (1972). *Z. Kristallogr.* **136**, 273–281.
Le Bail, A. (2008). *The Profile of a Bragg Reflection for Extracting Intensities*, In *Powder Diffraction Theory and Practice*, edited by R. E. Dinnebier and S. J. L. Billinge. Cambridge: RSC Publishing.
Marshall, A. T., Sunde, S., Tsypkin, A. & Tunold, R. (2007). *Int. J. Hydrogen Energy*, **32**, 2320–2324.
Pecharsky, V. K. & Zavalij, P. Y. (2009). *Fundamentals of Powder Diffraction and Structural Characterization of Materials*, 2nd ed. New York: Springer.

Petkov, V. (2008). *Mater. Today*, **11**, 28–38.
Petkov, V., Billinge, S. J. L., Shastri, S. D. & Himmel, B. (2000). *Phys. Rev. Lett.* **85**, 3436–3439.
Qiu, X., Thompson, J. W. & Billinge, S. J. L. (2004). *J. Appl. Cryst.* **37**, 678.
Reibenspies, J. H. & Bhuvanesh, N. (2006). *Powder Diffr.* **21**, 323–325.
Schmitt, B. & Bergamaschi, A. (2008). *Mythen II.* Paul Scherrer Institute, Switzerland.
Schmitt, B., Brönnimann, Ch., Eikenberry, E. F., Gozzo, F., Hörmann, C., Horisberger, R. & Patterson, B. (2003). *Nucl. Instrum. Methods Phys. Res. A*, **510**, 267–272.
Tucker, M. G., Dove, M. T. & Keen, D. A. (2000). *J. Phys. Condens. Matter*, **12**, L723–L730.
Von Dreele, R. B. (2006). *J. Appl. Cryst.* **39**, 124–126.
Wallwork, K. S., Kennedy, B. J. & Wang, D. (2007). *AIP Conf. Proc.* **879**, 879–882.